Electrochemical sensing and characterisation of aerobic marine bacterial biofilms on gold electrode surfaces

Journal:	*ACS Applied Materials & Interfaces*
Manuscript ID	am-2021-02669a.R2
Manuscript Type:	Article
Date Submitted by the Author:	n/a
Complete List of Authors:	Werwinski, Stephane; University of Southampton, Mechanical Engineering Wharton, Julian; University of Southampton, Mechanical Engineering Nie, Mengyan; University College London, UCL Institute for Materials Discovery Stokes, Keith; University of Southampton, Mechanical Engineering

SCHOLARONE™
Manuscripts

Electrochemical Sensing and Characterisation of Aerobic Marine Bacterial Biofilms on Gold Electrode Surfaces

Stephane Werwinski[a], Julian A. Wharton[a], Mengyan Nie[b], and Keith R. Stokes[a,c]

[a] National Centre for Advanced Tribology at Southampton (nCATS), School of Engineering, University of Southampton, Highfield, Southampton, SO17 1BJ, UK.
[b] UCL Institute for Materials Discovery, University College London, Malet Place, London, WC1E 7JE, UK.
[c] Physical Sciences Department, Dstl, Porton Down, Salisbury, Wiltshire, SP4 0JQ, UK.

Abstract

Reliable and accurate *in situ* sensors capable of detecting and quantifying troublesome marine biofilms on metallic surfaces are increasingly necessary. A 0.2 mm diameter gold electrochemical sensor was fully characterised using cyclic voltammetry in abiotic and biotic artificial seawater media within a continuous culture flow cell to detect the growth and development of an aerobic *Pseudoalteromonas* sp. biofilm. Deconvolution of the abiotic and biotic responses enable the constituent extracellular electron transfer and biofilm responses to be resolved. Differentiation of enhanced oxygen reduction kinetics within the aerobic bacterial biofilm are linked to enzyme and redox mediator activities.

Keywords: Marine biofilms; electrochemical; electron transfer; gold electrode; sensing.

Nomenclature

Symbol	Meaning	Unit
c	Concentration of a relevant species	mol cm^{-3}
D	Diffusion coefficient of a species	m^2 s^{-1}
E	Potential measured at the interface (*vs.* Ag/AgCl, 3.5 M KCl)	V
$E^{0'}$	Formal potential of the electrode converted into potentials (E *vs.* Ag/AgCl, 3.5 M KCl)	V
E_p	Peak potential (*vs.* Ag/AgCl, 3.5 M KCl)	V
E_pa	Anodic peak potential (*vs.* Ag/AgCl, 3.5 M KCl)	V
E_pc	Cathodic peak potential (*vs.* Ag/AgCl, 3.5 M KCl)	V
F	Faraday constant	96,485 C mol^{-1}
j	Current density	A cm^{-2}
j_p	Peak current density	A cm^{-2}
j_pa	Anodic peak current density	A cm^{-2}
j_pc	Cathodic peak current density	A cm^{-2}
k^0	Standard heterogeneous rate constant	cm s^{-1}
n_b	Number of generations between t_0 and t	dimensionless
Q_a	Anodic surface charge density	C cm^{-2}
r^2	Square of the sample correlation coefficient	dimensionless
R	Molar gas constant	8.314 J K^{-1} mol^{-1}
t	Time representative of the beginning of the stationary phase	h
T	Temperature of the solution	K
t_d	Average generation time	h
t_0	Time representative of the beginning of the exponential growth	h
t_1	Time representative of 0.080 V (*vs.* Ag/AgCl, 3.5 M KCl) in Eqn. 10	s
t_2	Time representative of 0.150 V (*vs.* Ag/AgCl, 3.5 M KCl) in Eqn. 10	s
V	Volume of solution	m^3
x	Cell density	cells mL^{-1}

1

| x_t | Cell density at t | cells mL^{-1} |
x_0	Cell density at t_0	cells mL^{-1}
z	Number of electrons involved in an electrochemical reaction	dimensionless
α	Transfer coefficient	dimensionless
α_a	Anodic transfer coefficient	dimensionless
α_c	Cathodic transfer coefficient	dimensionless
ΔE_p	Peak potential separation	V
μ_b	Specific growth of a bacterial species	h^{-1}
ν	Scan rate	V s^{-1}
$\nu^{1/2}$	Square root of the scan rate	V$^{1/2}$ s$^{-1/2}$

1. Introduction

Marine bacteria are ubiquitous and are the primary colonizers on metallic surfaces in seawater (*e.g.*, copper based and titanium alloys used in heat exchangers), plus they play a pivotal role in the biofilm development and the maintenance of a biofouling community [1]. The engineering issues of this troublesome phenomenon in naval applications and in merchant shipping are numerous and can cause excessive capital costs, for instance excess of £100k each to replace header castings [2]. Fouling affects the hydrodynamic properties (surface frictional resistance and causing flow restrictions) and reduces heat transfer performance of operating marine heat exchangers leading to frequent failures and blockages of fluid-handling components. In addition, marine microorganisms interact with metallic surfaces and can be involved in corrosion pathways through biocorrosion mechanisms [2,3]. Although the problems of biofouling in marine heat exchangers are abundant, suitable techniques capable of sensing for the presence and extent of biofilms on metallic surfaces are required. Likewise, proposed interfacial mechanisms attributed to aerobic biofilm action to enzymatic processes needs to be addressed [4,5]. Consequently, there is a focus on both smart sensing surfaces and early warning systems that quantitatively evaluate the metal/seawater interface and provide information of bacterial biofilm build-up.

Microbial biofilm electrochemical sensors exploit the electrode-biofilm interface as the sensing element, where the biofilm electrochemical activity provides the principle sensing strategy, as such a permeable biological membrane. Inert gold electrodes are often used to assess the electrochemical redox reactions involving oxidised and reduced species, and molecules, at the vicinity of the metallic interface. Fig. 1a shows a bacterial biofilm on a metallic surface with distinct bacterial clusters. Biofilms are composed primarily of microbial cells and extracellular polymeric substances (EPS), also known as extracellular polysaccharides [6]. Between 50% and 90% of the total organic carbon content is EPS [7]. The EPS is highly hydrated as it combines significant amounts of water within its structure by hydrogen bonding.
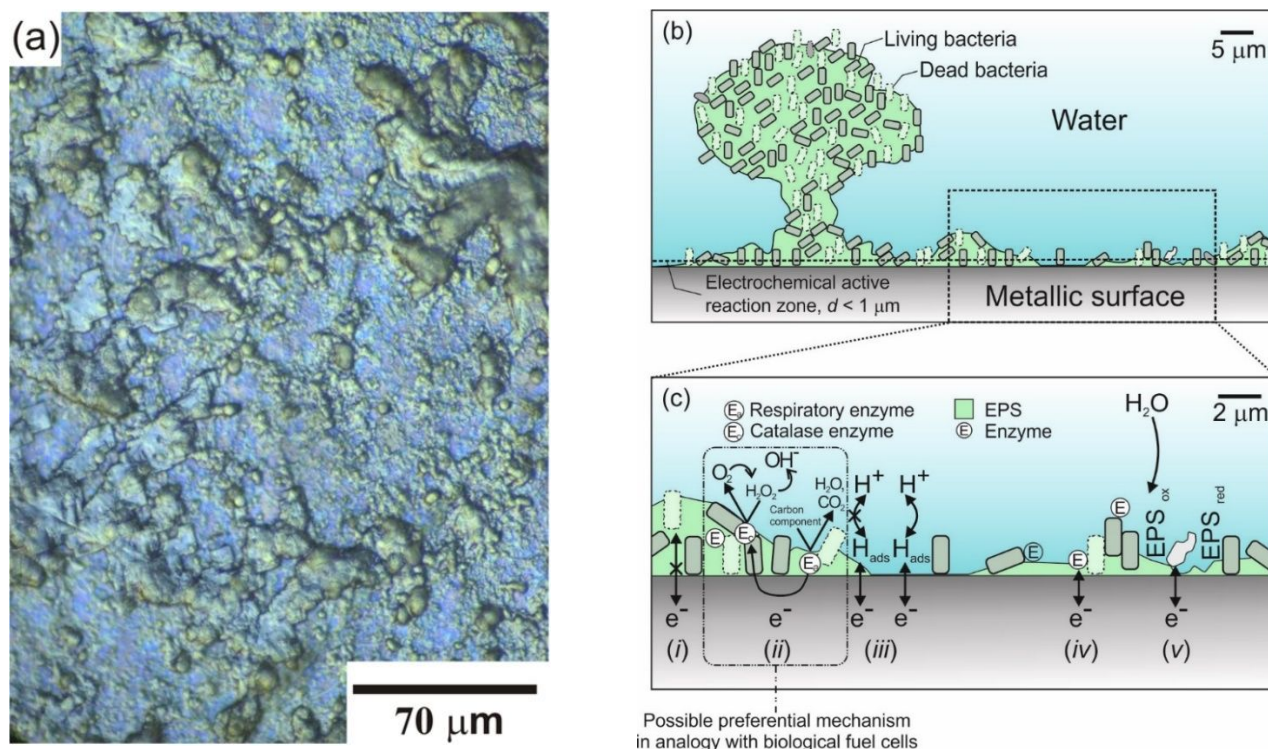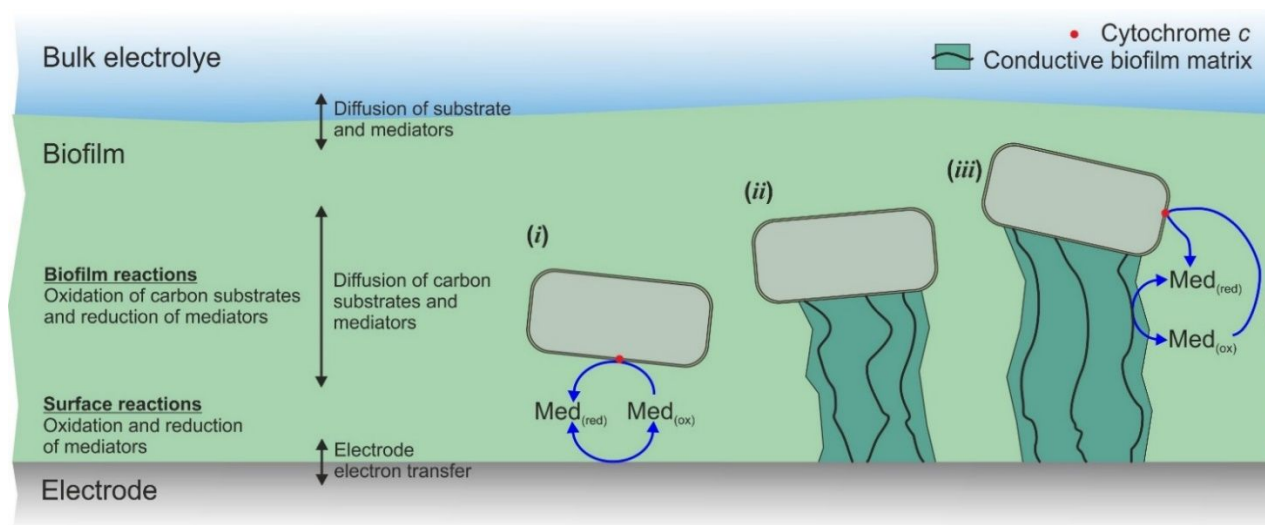
Fig. 1. Bacterial biofilm colonization: **(a)** a metallic surface immersed for 1 week in natural seawater at the National Oceanography Centre Southampton pontoon, **(b)** an overview of biofilm morphology, and **(c)** processes detected by electrochemical measurements, adapted from [8,9]. **(d)** Illustration of extracellular electron transfer: (*i*) diffusion-based EET, redox mediators that diffuse through the biofilm – acting as shuttles, reduced by the cell and can exchange electrons at the electrode surface; (*ii*) conduction-based EET with electrons transported via the conductive biofilm matrix to the electrode surface; (*iii*) mediator interaction in a conductive biofilm. It is speculated that redox mediators, such as flavin, can interact with outer membrane cytochrome *c* proteins, *e.g.*, MtrC and OmcA, receiving electrons from the periplasmic cytochrome MtrA and transferring them to terminal electron acceptors outside of the cell [4].

EPS composition and properties have marked effects [10]: (*i*) the composition and structure of the polysaccharides determine their primary conformation; and (*ii*) the EPS in the biofilm may vary

3

spatially and temporally. Some of these polysaccharides are neutral or polyanionic, as for the EPS of Gram-negative bacteria (such as *Pseudoalteromonas* sp.). The presence of either uronic acids or ketal-linked pryruvates confers the anionic property [10], allowing association of divalent cations such as calcium and magnesium that cross-link with the polymer strands and provide greater binding force in a developed biofilm [7]. Fig. 1b illustrates that bacterial biofilms consist of a heterogeneous structure of EPS matrix and bacteria cells randomly distributed on a metallic surface [1], thus inducing a range of electrochemical pathways and the mass transport near the metallic interface [8]. An expanded illustration of the metal/seawater interface shows the competing electrochemical processes, see Fig. 1c [8]. Direct electron transfer to redox active centres deep within the EPS matrix is not observed, see Fig. 1c(*i*). However, where the oxygen reduction reaction (ORR) is the prevailing reaction in neutral/alkaline conditions, enhancement mechanisms of the ORR by enzymatic processes have been proposed [11]. They are associated with enzymatic catalysis by aerobic microorganisms with the decomposition of an intermediate reactant (e.g., hydrogen peroxide – H_2O_2) resulting in an autocatalytic cycle through which the reduction current density is increased [11]. The exact nature of the ORR mechanism still remains to be fully determined. Analogous with biological fuel cell [9] – heterogeneous biofilm leads to the formation of galvanic cells – at sites with more positive potentials, where oxygen is deficient, soluble organic components in seawater are oxidized by respiratory enzymes forming H_2O and CO_2, see Fig. 1c(*ii*). Electrons transfer into the bacteria with subsequent charge transport inside the cell. As part of the redox process, electrons collect at sites with more negative potentials, where enzymatic assisted reduction of oxygen occurs at the outer biofilm areas, see Fig. 1c(*ii*). Whereas, hydrogen adsorption and reduction in Fig. 1c(*iii*) can be inhibited by the bacterial colonization of the surface [12,13]. After biocide treatments, a mechanism based on direct electron transfer to enzymes or other reductive agents entrapped in the EPS matrix may act as another pathway, see Fig. 1c(*iv*). Bacterial EPS has also been shown to be redox-active by allowing reductive and oxidative processes to occur, see Fig. 1c(*v*).

Overall, for long-range extracellular electron transfer (EET) two main mechanisms are discussed in the literature (illustrated in Fig. 1d): (*i*) diffusion-based and (*ii*) solid conduction matrix-based mechanisms [14,15,16]; however, the EET mechanism has rarely been effectively elucidated due to its complexity. EET is the process by which some microorganisms exchange intracellular electrons with an extracellular electron donor/acceptor, including naturally occurring compounds and artificial electrodes, across the cell membrane [17]. Diffusion-based EET is dependent on the migration, diffusion and/or advection of soluble redox mediators.

The aim of this study is to determine the electrochemical response of a 0.2 mm diameter gold sensor when exposed to abiotic and biotic test media and the influence of nutrients under aerated and deaerated conditions. Aerated and deaerated conditions are important in order to decouple the gold sensor electrochemical response when assessing the ORR in the presence of biofilm EPS, as well as to fully address the exploitation the sensing framework. The full consequences of potential interactions and interference are seldom reported in the published literature. This is the key novelty of this study. Experiments were designed to demonstrate the impact of redox mediators, both inorganic/organic and biological. The key objectives of this study were:
- to establish a framework for electrochemical sensing within abiotic and biotic artificial seawater (ASW) test media;
- to electrochemically detect marine bacterial biofilms and address the relevance of using electrical imposed polarization to monitor naturally occurring bacterial biofilms.

4

2. Materials and methods

2.1. Flow cell arrangement

Continuous culture flow cell systems are well-established methods for bacteria laboratory culture [18,19]. A modified once through flow cell device (5 mm × 5 mm × 40 mm) was designed to operate under a controlled low laminar flow condition ($R_e \approx 1$), see Fig. 2. In addition, the cell was under fully-developed flow conditions: with an entrance length of 0.33 mm for a 40 mm channel length, flow rate of 5.83×10^{-9} m^3 s^{-1}, wall shear stress of 0.31×10^{-3} Pa and a fluid residence time within the channel of 352 s. The overall system consists of a new approach to study initial bacterial biofilms development and extent under a controlled flow cell environment. The flow cell arrangement hosted three embedded flush electrodes for the electrochemical bacterial biofilm characterization (Fig. 2). The modified flow cell system had a 0.2 mm diameter polycrystalline gold (Au) working electrode mounted on the top surface, a silver/silver chloride (Ag/AgCl, 3.5 M KCl solution) reference electrode and a graphite counter electrode mounted on opposing sides in the rectangular flow channel. The Au electrodes were sealed under reduced pressure in a soda glass pipette using a heating coil before being embedded in the flow cell device. The Au and graphite electrodes were wet ground and polished to a final finish with 0.3 μm alumina powder, degreased in an ultrasonic bath, rinsed thoroughly in distilled water and then air dried using a Metaserv specimen dryer.
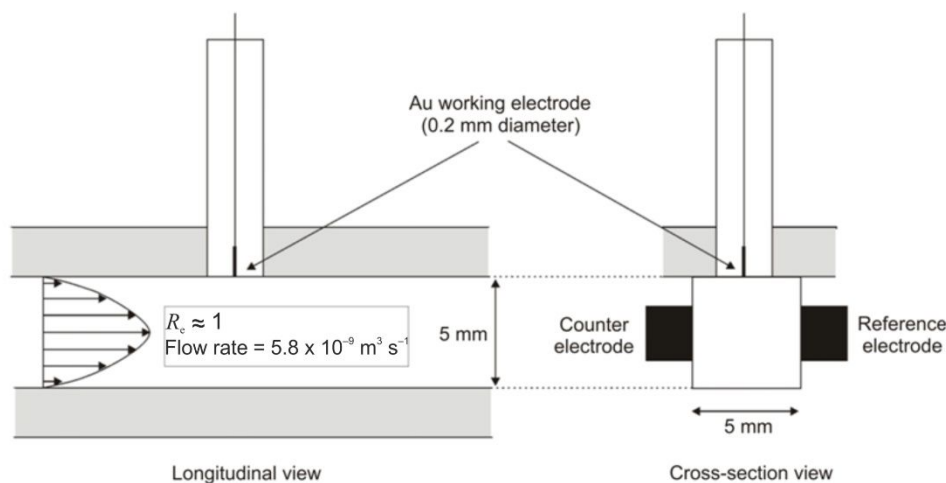
Fig. 2. Schematic of the flow cell electrode arrangement for the electrochemical measurements.

2.2. Electrochemical measurements

Cyclic voltammetry (CV) at a scan rate of $v = 0.200$ V s^{-1} in N$_2$ deaerated 1 M H$_2$SO$_4$ was used to characterize the surface state of the Au electrode. CV at $v = 0.100$ V s^{-1} of the Au electrode in a 3.5 wt.% NaCl solution was performed periodically or at 72 h (three days) under continuously air and N$_2$ sparging, aerated and deaerated conditions, respectively, to support the analysis of the cyclic voltammogram in the ASW media. Sparging with N$_2$ changed the bulk DO level, *i.e.*, 6.90 and 0.20 ppm between the aerated and deaerated conditions. In addition, CV at $v = 0.100$ V s^{-1} was utilized to electrochemically characterize the Au electrode in the abiotic and biotic media. A stable CV response was generally obtained between three and five cycles. For clarity, all potentials are reported with respect to silver/silver chloride (Ag/AgCl, 3.5 M KCl) reference electrode system ($E_{\text{Ag/AgCl, 3.5 M KCl}}$ *vs*

5

. SHE = +0.205 V). As part of the three-electrode setup a graphite counter electrode was used. All electrochemical tests were performed with Gamry Reference 600 within a Faraday cage in order to minimize interference due to external electromagnetic fields and light irradiance. The light irradiance (inside the Faraday cage) was measured at 0.12 ± 0.01 µmol photons m^{-2} s^{-1} using a Li-Cor Li-189 Photometer.

2.3. *Pseudoalteromonas culture*

A marine aerobic, bacterium *Pseudoalteromonas* sp. strain NCIMB 2021 was obtained from the National Collection of Industrial, Marine and Food Bacteria (NCIMB) in Aberdeen, UK. *Pseudoalteromonas* is a genus of Gram-negative marine bacteria, found in the open-ocean and coastal seawaters, and characterised as straight rods (2-3 µm) with a single polar flagellum, sheathed or unsheathed for motility and utilising carbon substrates: carbohydrates, alcohols, organic acids and amino acids [20,21,22]. A new culture was resuscitated from a freeze-dried ampoule, and sub-cultured twice in 20 mL solid agar NCIMB medium 210 using sterile Petri dishes at 18 ± 1°C over 72 h. A continuously aerated and stirred sterile standard batch culture containing 250 mL agar NCIMB medium 210 was then used to prepare 200 µL aliquots of 2 h-old *Pseudoalteromonas* culture (inoculum) for the electrochemical experiments. The 1 L pH 7.3 agar solution contained: 3.0 g of yeast extract, 5.0 g of tryptone, 15.0 g agar, 750 mL of 0.22 mm filtered aged seawater (seawater from Solent Water, Southampton kept in the dark in sterile glass bottles for between 3 and 4 months at a controlled temperature of 6 ± 1°C) and 250 mL deionised water (18.2 MΩ cm, Milli-Q). Similarly, the bacterial cell populations were evaluated using a FACsort marine flow cytometer (argon source at λ = 488 nm) by sampling at different time intervals (*i.e.*, 0 h, 4 h, 21 h and 72 h, respectively) within the standard batch culture and the flow cell to address any microbiological variability. Each sample contained: 500 µL test solution, 5 µL DNA-stain SYBR Green I (Sigma-Aldrich) at a ratio of 1:100, 50 µL potassium citrate solution at a ratio 1:10 and 25 µL of bead stock solution (1,125,485 beads per mL). In particular, two series of three samples, diluted 10 and 100 times, were prepared to ensure measurements accuracy from the flow cytometer. A 1 % final concentration paraformaldehyde was used in each sample as a fixative to kill *Pseudoalteromonas* sp. cells and preserve their membranes. All the samples were mixed using a vortex and then stored at –20°C. Prior to performing the flow cytometry measurements, all the samples were defrosted at 35°C for about 5 – 10 minutes.

2.4. *Test media*

The freshly prepared, 0.22 µm filtered and flush test solutions in Table 1 were 3.5 wt.% NaCl solution at pH 8.0, abiotic ASW and ASW with a single aerobic *Pseudoalteromonas* sp. strain NCIMB 2021. The abiotic ASW at a pH 8.1 contained dissolved salts and metal-ions, vitamins and nutrients (carbon substrates), see Supporting information Table S1 [23]. In addition, 0.1 % (w/v) tryptone and 0.07 % (w/v) yeast extract were added to enhance the ASW organic carbon content relevant to open seawater conditions resulting in a similar test condition to [24]. Alternatively, a control ASW test solution was used consisting of dissolved salts and metal ions, and also ethylenediaminetetraacetic acid (EDTA) to keep metal ions in solution (Table S1). All the prepared solutions were made using deionised water (18.2 MΩ cm, Milli-Q). It is worth noting there are reported complexities in using yeast extract, since its constituents are redox mediators, adsorb onto electrode surfaces and chelate metal ions [25] and the test matrix was designed to highlight any significant interference.

Table 1. Biochemical characteristics of the test media

Test media	Biochemical characteristics	Experimental details
1. 3.5 wt.% NaCl at pH 8.0	Organic free –sterile	Baseline for the ORR (3.5 wt.% NaCl)
2. 0.1 % (w/v) tryptone and 0.07 % (w/v) yeast extract in ASW at pH 8.1	Organic nutrients – sterile – abiotic	Baseline for a conditioning film (adsorbed organic layer) (Abiotic ASW)
3. Control ASW test solution at pH 8.1	EDTA – sterile – abiotic	Baseline for complex metal-ions (Control ASW)
4. 0.1 % (w/v) tryptone and 0.07 % (w/v) yeast extract in ASW with 200 µL aliquot of 2h-old *Pseudoalteromonas* sp. Strain NCIMB 2021 culture at pH 8.1	Organic nutrients – non-sterile – Biotic	Biofilm (Biotic ASW)

It should be noted that although the seawater composition by Riegman *et al.* has often been used in the research literature, the sodium bicarbonate ($NaHCO_3$) concentration is twice as high compared with natural ocean and artificial seawaters [26]. The Riegman growth environment corresponds to a nutrient-replete condition (as opposed to a nutrient-limited condition), thus favouring the exponential growth of marine microorganisms, such as diatoms and heterotrophic bacteria.

Compared to the abiotic ASW and ASW with *Pseudoalteromonas* sp. media, the 3.5 wt.% NaCl test solution was free of organic matter and is more representative of a sterile condition, and also a useful control test to assess the ORR in alkaline conditions [23]. In addition, compared to the ASW with *Pseudoalteromonas* sp. medium, the abiotic ASW was free of living organisms but still contained organic matter, which had passed through the 0.22 µm filter. Thus providing a baseline for adsorbed organic material (conditioning film) on the Au surface [1,2]. Whereas the *Pseudoalteromonas* sp. inoculated in ASW represented a more complex biochemical medium, which contained organic material and living organisms (biotic). The physicochemical properties of the test media in Table 1: conductivity, dissolved oxygen (DO), pH and temperature were assessed before and after each test, allowing any variations to be identified. The conductivity (approx. 50 mS cm^{-1} at 22°C), DO level ($\approx$6.90 parts per million, ppm), and pH (8.0 ± 0.2) of the test media were measured using an ATI Orion model 162 conductivity meter, a Hanna Instruments HI9145 DO probe with the media flowing at about 0.3 m s^{-1} and a Hanna Instruments HI98129 Combo probe, respectively. All experiments were performed under temperature controlled conditions at 18 ± 1°C. Overall, the test media physicochemical properties were representative of surface sea waters from the North Atlantic equilibrated with the atmosphere [27]. The media were checked regularly for turbidity over the test duration; all remaining transparent and thus indicated the absence of backflow and no contamination.

2.5. Confocal microscopy characterisation

Confocal microscopy (Leica TCS SP2) studies utilizing a molecular probe method Live/Dead *Bac*Light™ (from Invitrogen Ltd, Paisley, UK) were performed *ex situ* using an excitation wavelength of 470 nm for assessing the morphology and distribution of bacterial colonies, the presence of EPS matrix on the Au surface. *Bac*Light is composed of a green-fluorescent SYTO® 9 stain, which penetrates intact cells – alive and/or dead and a red-fluorescent propidium iodide stain for dead or dying cells with damaged membranes only. A series of stacks of confocal images were collected with the Leica TCS SP2

at 0.5 µm intervals along the *z*-direction. Using Leica Confocal Software (LCS) version 2.61 the stacks of the confocal images were projected allowing biofilm thickness to be assessed.

3. Results and discussion

3.1. *Pseudoalteromonas sp. growth curve*

Fig. 3 shows the 53 h (2.2 days) growth curve of the *Pseudoalteromona*s sp. Each data point is the mean number of cells detected per mL in the non- and diluted samples, *i.e.*, corrected for the 10 and 100 dilution factors.
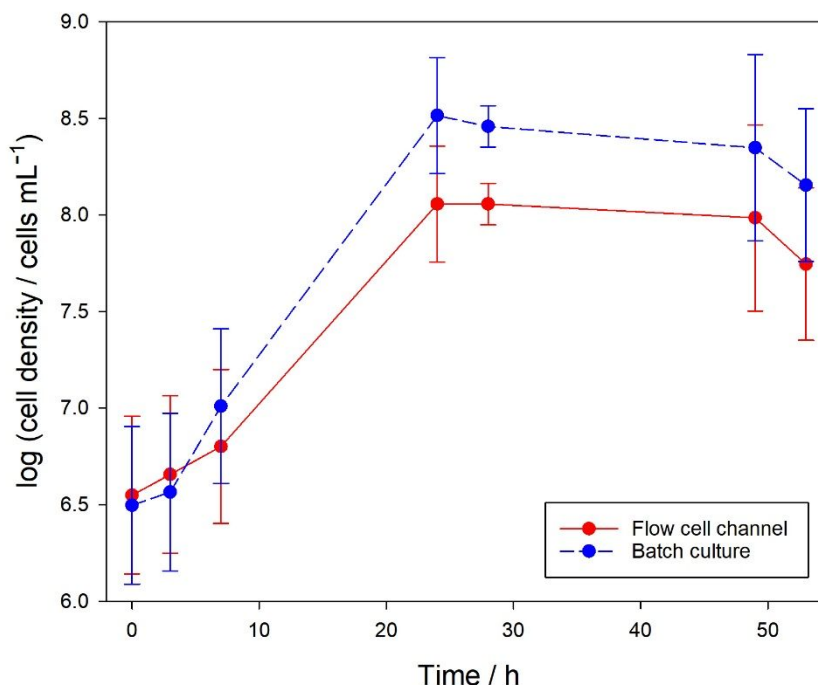
Fig. 3. Bacterial growth curve for *Pseudoalteromonas* sp. NCIMB 2021: **(dashed line)** cultured in the 250 mL batch culture and **(solid line)** established inside the flow channel. Bacterial cell populations were evaluated using a FACsort marine flow cytometer (argon source at λ = 488 nm).

The Fig. 3 error bars result from the 10× and 100× dilution correction, which affects the overall measurement precision. After a 53 h exposure, the presence of biological by-products in the samples limited the measurable/detectable signal, thus there were no further measurements beyond 53 h. The growth curves for both batch and flow cell cultures (*i.e.*, logarithmic, stationary and senescence phase) were generally similar to typical bacterial growth plots [3,28]. Initially, within the first 3 h, the flow cell and batch culture bacterial growths are nominally similar at approximately 3.5×10^6 cells mL^{-1}. However, during the logarithmic growth phase the flow cell bacterial growth was marginally lower than the batch culture as a consequence organic carbon nutrients being more readily available and thus favouring higher bacterial growth in the batch culture than for the flow cell channel. The bacterial cell populations between 1.0×10^8 and 3.2×10^8 cells mL^{-1} during the plateau phase (24 to 49 h) agree with data reported by Fletcher, *i.e.*, stationary and senescence phase were reached at 21 – 22 h and between 45 and 50 h, respectively (with 2.5×10^9 to 5.0×10^9 cells mL^{-1}) [24].

From Fig. 3, it is possible to assess the growth rate (μ_b in h^{-1}) using Eqns. 1 and 2 [29]:

$$t_d = \frac{\ln 2}{\mu_b} \qquad\qquad \text{......(1)}$$

$$n_b = \frac{\log x_t - \log x_0}{\log 2} \text{ for } n_b \text{ generations (i.e., } n_b t_d\text{) between } t_0 \text{ and } t \qquad \text{......(2)}$$

where t_d is the doubling time or mean generation time in hours (h). It represents the average time required for all the components of the culture to double. In addition, x_0 and x_t denote the cell density at t_0 and t, which represent of the start of the logarithmic growth and stationary phase, respectively.

Table 2. Biological parameter evaluation for the batch culture and flow cell systems between $t_0 = 3$ h and $t = 24$ h (data from Fig. 3)

| Biological parameters	Batch culture	Flow cell
$\log x_0$ (at 3 h)	6.56	6.65
$\log x_t$ (at 24 h)	8.51	8.06
x_0 (at 3 h) / cells mL^{-1}	3.68×10^6	4.53×10^6
x_t (at 24 h) / cells mL^{-1}	3.27×10^8	1.14×10^8
Generations, n_b	6.48 generations in 21 h	4.65 generations in 21 h
Doubling time, t_d (i.e., $21/n_b$) / h	3.24	4.52
Growth rate, μ_b/ h^{-1}	0.21	0.15

Table 2 summarizes the biological parameters of both the batch and flow cell culturing systems in terms of mean generation time and growth rate. In this instance, for the flow cell data between 3 and 24 h: x_0 = 4.53×10^6 cells mL^{-1} and x_t = 1.14×10^8 cells mL^{-1}, there are $(8.06 - 6.65)/\log(2)$ = 4.65 generations within 21 h. The mean generation time and growth rate are 4.52 h and 0.15 h^{-1} for the flow cell, 3.24 h and 0.21 h^{-1} for the batch culture, respectively, which were within the same order of magnitude. These growth rates can be related to typical μ_b for standard batch culturing vessels (i.e., $0.5 - 0.7$ h^{-1} [30] or biofilm model system operating at a fast dilution rate of 0.2 h^{-1}, which are usually about 10 times higher than that for typical dilution rates using a chemostat (i.e., roughly 0.05 h^{-1}) [29]. As a result, the growth rate of 0.15 h^{-1} was deemed acceptable for the current study.

It is important to establish the microbial growth kinetics before undertaking tests utilising biotic media, in order to assess whether a particular bacterial strain is adapted to metabolise certain nutrients/substrates. The microbial growth curve reflects the bacterial population when grown in a closed system of microbial culture of fixed volume (i.e., batch culture). The typical growth curve for a population of cells can be divided into distinct phases: the lag phase, log phase, stationary phase, and death phase. Fig. 3 and Table 2 demonstrate only minor differences in the bacterial growth curves for the flow cell and batch culture, with comparable doubling times and growth rates. Hence, there is a negligible effect when using either the flow cell or batch culture setups. Additionally, the growth curve characterisation of the *Pseudoalteromonas* strain shows the flow cell setup is a suitable culturing system, thus allowing microbial fouling colonisation and development.

3.2. Overview of the cyclic voltammograms

Metallic surfaces for marine application are subject to degradation due to the presence of damaging chloride species and the formation of corrosion products (hydrated oxides), leading to oxide fouling of the metallic interface. Ideally, the sensing surface is inert to ensure stability of the sensing area and reliability of the electrochemical response. Gold electrodes are often used in microbiology for their biocompatibility. Nonetheless, it is important to first fully characterise the fundamental electrochemical performance in abiotic conditions. A cyclic voltammogram performed using deaerated 1 M H_2SO_4 was made in order to characterize and corroborate the behaviour of the 0.2 mm diameter gold (Au) electrode (see Fig. 4a) with reported Au voltammograms in 1 M sulphuric acid [31,32,33]. The extended region (*A*) between +0.900 and +1.350 V represents the Au oxide formation, $Au(OH)_3/Au_2O_3$, see Eqns. 3 and 4.

$$Au + 3H_2O \rightarrow Au(OH)_3 + 3H^+ + 3e^- \quad E = +1.245 \text{ V} \qquad \text{......(3)}$$
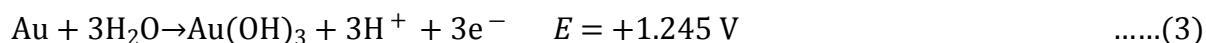
where the product $Au(OH)_3$ is the hydrated oxide,

$$2Au + 3H_2O \rightarrow Au_2O_3 + 6H^+ + 6e^- \quad E = +1.305 \text{ V} \qquad \text{......(4)}$$
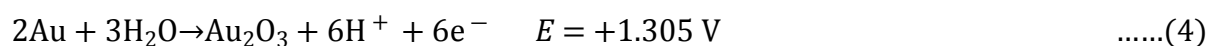
Here the product Au_2O_3 is the anhydrous oxide.

The anodic peak feature (*A*) between +0.900 V and +1.350 V are consistent with the formation of an oxide monolayer at the Au surface [31]. The hysteresis, *i.e.*, the difference in the potential range between peaks for oxide formation and reduction in regions (*A*) and (*B*), is attributed to gradual changes in the oxide film. Dipolar ($Au^{\delta+}.OH^{\delta-}$) species are produced during oxide growth (the positive potential sweep), covering the gold surface. The oxide coverage of the gold surface increases the electrostatic repulsion energy favourable for additional dipoles generation in the extended region (*A*).

The reduction peak (*B*) around +0.550 V is not well-defined. This is unusual since a conventional Au electrode voltammogram should ideally exhibit a sharp cathodic peak. A possible explanation could be the incomplete release (during the negative sweep) due to lateral repulsion or stress in the surface layer of the polished gold electrode [31]. Ideally for a complete reduction of the electrostatic repulsion barrier, the post-electrochemical process of the Au oxide formation is governed by place-exchange reaction, *i.e.*, rotation of surface dipoles resulting in the release of lateral residual stresses in the surface layer [31]. Overall, the electrochemical response for the 1 M sulphuric acid in Fig. 4a was typical for a gold-acid voltammogram [31], *i.e.*, gold oxide formation/reduction at (*A*) and (*B*).

(a)

(b)
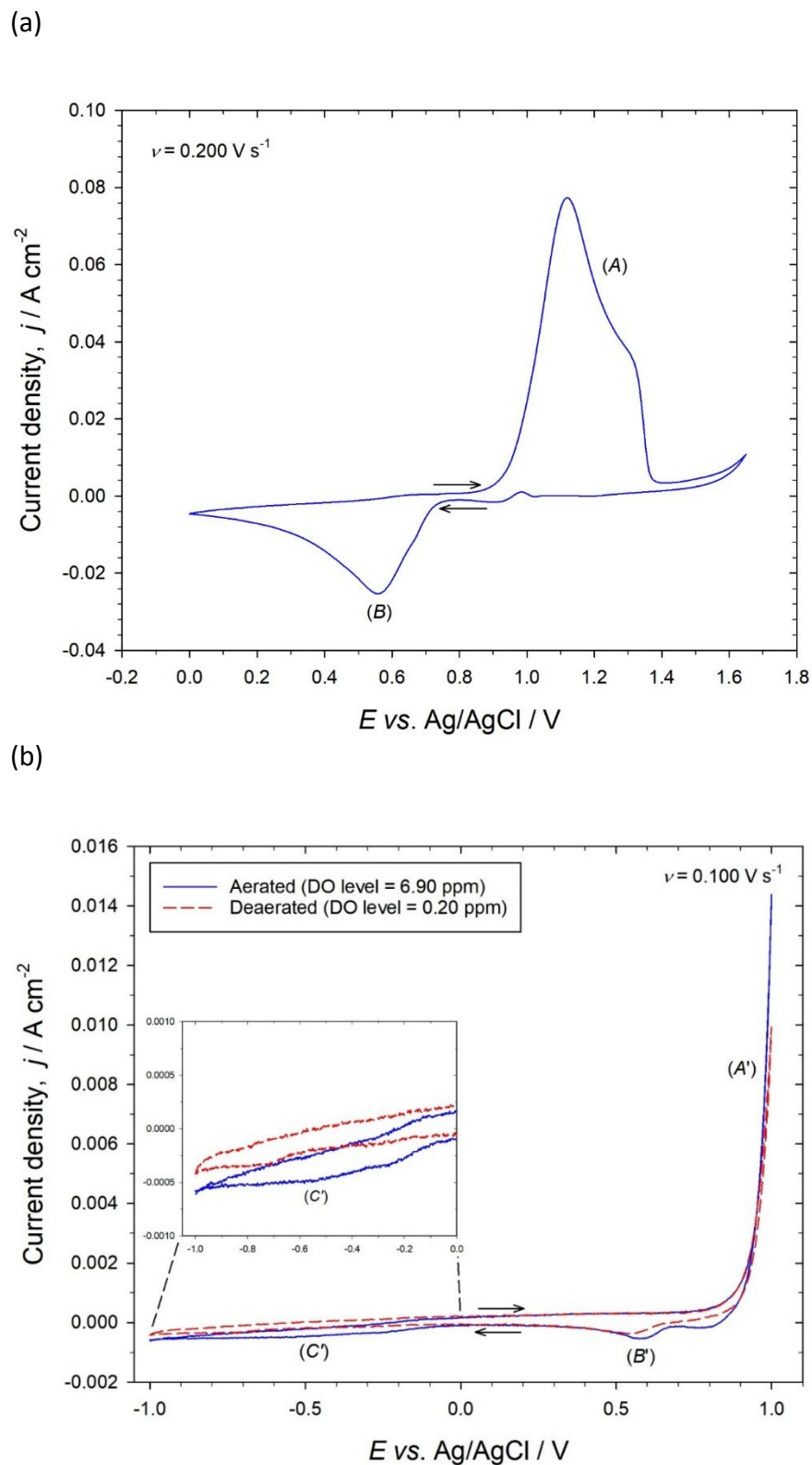
Fig. 4. **(a)** Cyclic voltammogram for a 0.2 mm diameter Au electrode in N_2 deaerated 1 M H_2SO_4 at a scan rate of 0.200 V s^{-1}. **(b)** Comparison of cyclic voltammograms for a 0.2 mm diameter gold electrode in N_2 deaerated (dashed line) and aerated (solid line) 3.5 wt.% NaCl (test medium #1) at a scan rate of 0.100 V s^{-1}.

11

3.3. CV for test medium #1 (*sterile - organic nutrient free*)

For clarity, only the 72 h data is presented in Fig. 4b. For the entire test duration, cyclic voltammograms were found to be time-independent for the NaCl test solution. The time-independent response is attributed to no modification of the overall electrode kinetics at the Au/3.5 wt.% NaCl interface. At electropositive potentials, the Au oxidation (*A'*) begins at around +0.750 V. The presence of chloride ions (Cl^-) also affects the gold dissolution kinetics, in parallel to the gold oxide film formation, leading to the formation of tetrachloroaurate ions ($AuCl_4^-$).

$$Au + 4Cl^- \rightarrow AuCl_4^- + 3e^- \quad E = +0.797 \text{ V} \quad\quad\quad ......(5)$$

As part of the gold oxide film formation, the surface will be covered by various species, such as $Au(OH)$, $Au(OH)_3$ or $AuO(OH)$. An associated marked cathodic (stripping) peak of the gold oxide in region (*B'*) around +0.550 V is not evident in Fig. 4b, thus indicative of an essentially irreversible process [34]. From the Pourbaix diagram for the gold/chloride-water system in Supporting Fig. S1, two possible reaction pathways can be deduced to better assess the gold oxide removal mechanism.

In the first reaction pathway, gold may undergo a dissolution in the presence of Cl^- to form a soluble $AuCl_2^-$ complex. The $AuCl_2^-$ stability depends on the chloride and gold activity ratios (stable at higher values). With a chloride deficiency at the gold/solution electrode interface, $AuCl_2^-$ can undergo disproportionation to simultaneously form both Au and $AuCl_4^-$, as expressed in Eqn. 6.

$$3AuCl_2^- \rightarrow 2Au + AuCl_4^- + 2Cl^- \quad\quad\quad ......(6)$$

The second reaction pathway is where gold dissolution in a NaCl solution can proceed by the reaction of $Au(OH)_3$ with Cl^- to form mixed chlorohydroxo Au complexes, such as $AuCl(OH)_3^-$.

$$Au(OH)_3 + Cl^- \rightarrow AuCl(OH)_3^- \quad\quad\quad ......(7)$$

A further exchange of hydroxyl ligands of the $AuCl(OH)_3^-$ complex can occur to yield $AuCl_4^-$.

The well-established ORR on gold proceeds only via an intermediary mechanism, with H_2O_2 as the reactant intermediate [35-39]. This is often attributed to the relatively poor catalytic performance of gold for the decomposition of H_2O_2 compared with platinum. In alkaline solutions, oxygen is readily reduced to H_2O_2 (Eqn. 8) and only partial peroxide reduction to water occurs on the gold surface.

$$O_2 + 2H_2O + 2e^- \rightarrow H_2O_2 + 2OH^- \quad E = -0.351 \text{ V} \quad\quad\quad ......(8)$$
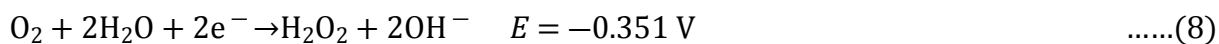
The feature at (*C'*), between –0.200 V and the plateau at –0.700 V, shows clear differences between the deaerated and aerated NaCl solution (#1), demonstrating a well-defined ORR wave governed by Eqn. 8 for the aerated condition (solid line, Fig. 4b). The ORR appears to be potential independent and reaches mass transport limited current in the observed potential range. Although the element steps of ORR are still in debate, it is generally believed that the reduction of O_2 to H_2O_2 is determined by a chemical step involving the adsorbed peroxide species [35,36].

The second step with adsorbed peroxide species, which corresponds to a second wave of ORR that is poorly defined in Fig. 4b (solid line), can be equivalent to Eqn. 9:

$$H_2O_2 + 2e^- \rightarrow OH^- \qquad\qquad\qquad\qquad ......(9)$$

The electrochemical response in Fig. 4b with gold oxide formation and stripping at electropositive potentials (plus an ORR wave in the electronegative potentials) agrees with the reported gold behaviour in a 3.5 wt.% NaCl test solution and is summarised in Table 3. Importantly, a cathodically polarised gold electrode, between –0.200 V to the plateau at –0.700 V, can be used to monitor the ORR, which is fundamentally the working principle of the Clark electrode [40,41], whereas more positive potentials can provide key insights into possible self-cleaning/regeneration of the Au electrode surface when used in-service [42,43,44].

Table 3. Detectable electrochemical processes at the Au/3.5 wt.% NaCl interface (test medium #1) over a potential range between –1.000 and +1.000 V (*vs.* Ag/AgCl, 3.5 M KCl)

Potential	Region	Description	
$\geq$ +0.750 V	(A')	Au oxide formation	Self-cleaning of the Au surface
Around +0.550 V	(B')	Cathodic stripping of the Au oxide	
Between –0.200 V to the plateau at –0.700 V	(C')	ORR wave	

3.4. CV for test medium #2 (*abiotic condition –sterile organic components*)

Fig. 5a shows the CV for the 72 h data since there was a time-independent response for the abiotic test medium #2 (containing organic components), which is consistent with the NaCl test medium #1 (Fig. 4b). Again, there was no attributable modification of the electrode kinetics at the gold/abiotic ASW interface with time.

In Fig. 5a, for the ASW (test medium #2 – sterile with soluble carbon substrates), peaks (A') and (C') indicate gold oxide formation and the ORR, and were thus consistent with the behaviour shown in Fig. 4b. Additional oxidation and reduction peaks at (A'') and (B'') are apparent for the abiotic ASW at ±0.125 V, which are likely to be associated with the redox of inorganic species. Plus, an oxidation wave at (C'') between +0.500 V and +0.900 V was more pronounced for the aerated ASW medium (Fig. 5a), as observed by Hu *et al.* using a similar organic medium [45]. Fig. 5b provides a direct comparison with the aerated ASW response (#2) and sterile NaCl solution (#1), and is overall indicative of the interfacial changes: inorganic species adsorption/desorption processes at (A'') and (B'') and the oxidation of organic material (favoured in aerated conditions) at feature (C''). Likewise, regions (A') and (B') linked to gold oxide formation and stripping for the abiotic ASW were less prominent and were shifted/suppressed due to the presence of adsorbed organic components on the gold surface [46,47,48].

(a)

(b)

(c)

(d)
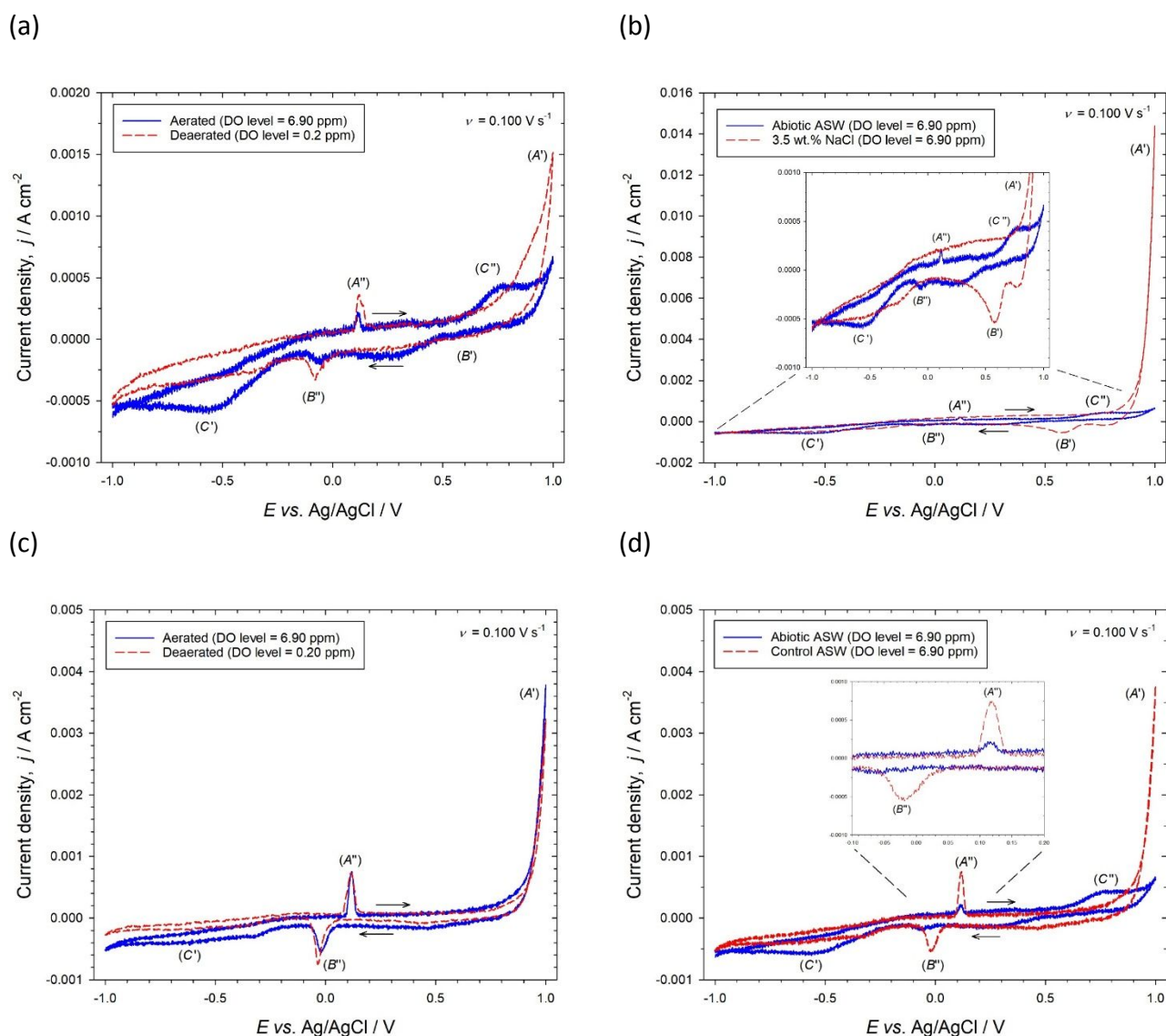
Fig. 5. **(a)** Comparison of cyclic voltammograms for a 0.2 mm diameter Au electrode in N_2 deaerated (dashed line) and aerated (solid line) abiotic ASW (test medium #2) at a scan rate of 0.100 V s^{-1} after 72 h. **(b)** Direct comparison of cyclic voltammograms for a 0.2 mm diameter Au electrode in aerated 3.5 wt.% NaCl (test medium #1 – dashed line) and abiotic ASW (test medium #2 – solid line) at a scan rate of 0.100 V s^{-1} after 72 h. **(c)** Comparison of cyclic voltammograms for a 0.2 mm diameter Au electrode in N_2 deaerated (dashed line) and aerated (solid line) control ASW (test medium #3) at a scan rate of 0.100 V s^{-1} after 72 h. **(d)** Direct comparison of cyclic voltammograms for a 0.2 mm diameter Au electrode in aerated control (test medium #3 – dashed line) and abiotic (test medium #2 – solid line) ASW at a scan rate of 0.100 V s^{-1} after 72 h.

To explore the nature of the abiotic ASW electrochemical response, an additional complementary study using the control ASW (test medium #3 –only inorganic species, plus EDTA) and compared with aerated abiotic ASW (test medium #2) is shown in Figs. 5c and 5d. The control ASW CV (Fig. 5c) gave a response similar to abiotic ASW (Fig. 5a) with distinct regions (*A'*), (*C'*), (*A''*) and (*B''*) representative of the gold oxide formation, the ORR wave and the oxidation/reduction peaks (identical to the abiotic ASW test medium – confirming the redox of inorganic species) due to the electroactive adsorption/desorption of inorganic ions. In contrast, the ORR wave in region (*C'*) was more evident for the abiotic ASW when compared with 3.5 wt.% NaCl (test medium #1, Fig. 5b) and the control ASW

(Fig. 5d), suggesting enhanced reduction kinetics when an adsorbed organic layer (conditioning film) is present on the gold surface [45]. Similarly, oxidation and reduction peaks of inorganic species (A'') and (B'') in Fig. 5d were depressed for the abiotic ASW, which is likely to be associated with the physical blocking effects of adsorbed organic components (the exposed gold surface area is reduced) [46,48]. The oxidation wave (C'') was more pronounced when compared with the control ASW medium, which can be attributable to the oxidation of organic components and consistent with [45]. It should be noted that the organic components in the sterile ASW (medium #2) are B vitamins that are known to act as redox mediators [25]. The enhanced reduction kinetics linked to the presence of an organic conditioning film, in which organic molecules (mainly B vitamins and EDTA) can form a loosely packed monolayer on the gold surface, where discontinuities allow mass transport of oxygen to continue [45].

From Fig. 5d, the anodic surface charge density (Q_a) in the region (A'') can be evaluated by integrating the area under the curve between +0.080 V and +0.150 V.

$$Q_a = \int_{t_1}^{t_2} j \, \mathrm{d}t \qquad\qquad\qquad\qquad ......(10)$$

where t_1 and t_2 are the times representative of +0.080 and +0.150 V, respectively.

The cathodic peak in region (B'') for the abiotic ASW in Fig. 5d was poorly defined (thus, not considered for percentage surface coverage studies), linked to the influence of oxygen, *i.e.*, a peak shift towards the ORR region (C') [46]. Table 4 shows the Q_a using Eqn. 10 and the corresponding percentage surface coverage for the adsorbed organic components.

Table 4. Summary of surface charge density (Q_a) for the region (A'') in Fig. 5d and the corresponding percentage surface coverage of adsorbed organic layers

Peak of interest (A'')	Control ASW (#3)	Abiotic ASW (#2)
Q_a / C cm^{-2}	1.25×10^{-2}	3.70×10^{-3}
Percentage surface coverage of adsorbed organic layers	Roughly 70 %	

Approximately 70 % surface coverage was assessed for the adsorbed organic layer (conditioning film), which can suppress the electron transfer process at the gold surface [46,48,49]. Overall, this represents a limited electrochemical interpretation of the surface coverage occurring when a conditioning film forms on the gold surface. Consequently, corroborative tests such as atomic force microscopy and spectroscopy methods on gold electrodes would be useful to gain insights on the exact nature, composition and morphology of the adsorbed organic layer [50].

In addition, cyclic voltammograms for the deaerated and aerated control ASW (test medium #3), and also abiotic ASW (test medium #2), were performed at scan rates of 0.050, 0.100, 0.200 and 0.500 V s^{-1}. This allows electron transfer processes of inorganic species redox peaks (A'')/(B'') (Fig. 4d) to be further studied (see Eqn. 11 [46,51] using plots of the absolute anodic and cathodic peak current

15

density, $|j_{pa}|$ and $|j_{pc}|$ vs. $v^{1/2}$, where j_{pa} and j_{pc} correspond to the magnitude of the anodic and cathodic peaks.

$$j_p = (2.99 \times 10^5)z\alpha^{1/2}cD^{1/2}v^{1/2} \qquad \qquad ......(11)$$

here j_p is the peak current density, α the transfer coefficient, c and D the concentration and the diffusion coefficient of the relevant species. Eqn. 11 is strictly only valid for reversible systems and plots should pass through the origin point. For simplicity, only the plots $|j_{pa}|$ and $|j_{pc}|$ vs. $v^{1/2}$ for the aerated conditions are presented in Supporting Figs. S3 and S4 (similar trends are obtained for the nitrogen deaerated ASW media). A linear relationship is clearly evident between $|j_p|$ and $v^{1/2}$ for the control ASW (r^2 = 0.99) in contrast with the abiotic ASW (r^2 = 0.93), where current densities were five-fold lower than for the control ASW. This demonstrates a diffusion dominant process is associated with the inorganic species redox peaks (A'')/(B'') (Fig. 5d). The observed five-fold reduction of current density obtained in abiotic ASW in comparison to the control ASW is due to the surface blockage caused by adsorption of organic materials and is in good agreement with the estimated surface coverage of roughly 70 %, (Table 4).

For the inorganic species redox peaks (A'')/(B'') the ratio of $|j_{pa}|$ to $|j_{pc}|$ is close to 1, thus revealing a quasi-reversible electron transfer process [46]. In addition, for the aerated control ASW (test medium #3), the anodic and cathodic peaks shift positively and negatively, respectively, with increasing scan rate, see Supporting Table S2. The peak-to-peak separation, $\Delta E_p = E_{pa} - E_{pc}$, ranged between 0.117 V and 0.184 V, which is much greater than the theoretical 0.059 V for a single electron transfer reaction. The difference between the experimental and the theoretical prediction further confirms the quasi-reversible characteristic of electron transfer reaction, which could be ascribed to the presence of organic component (D-biotin, thiamine and cyanocobalamine) and EDTA amide ligands bound to the gold surface, thus forming coordinated metal ion complexes with an additional solution resistance. The single electron transfer process for inorganic redox peaks (A'')/(B'') can be attributed to the ferric-EDTA complex (Eqn. 12) [52,53,54], where the concentration of $FeCl_3$ is similar to EDTA in Supporting Table S1.

$$Fe^{3+}(EDTA) + e^- \rightarrow Fe^{2+}(EDTA) \quad E = -0.085 \text{ V} \qquad \qquad ......(12)$$
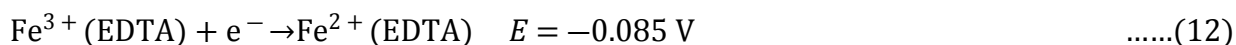
For an irreversible one-step, one-electron electrochemical system the anodic and cathodic transfer coefficients (α_a and α_c) can be determined utilising the relationships E_{pa} and E_{pc} vs. $\ln v$ (Eqn. 13) [39,44] for the aerated control ASW in Supporting Fig. S5.

$$E_p = E^{0'} + \frac{RT}{\alpha F}\left[0.780 + \ln\left(\frac{D^{1/2}}{k^0}\right) + \ln\left(\frac{\alpha F v}{RT}\right)^{1/2}\right] \qquad \qquad ......(13)$$

where E_p is the peak potential, $E^{0'}$ is the formal potential of the electrode and k^0 the standard heterogeneous rate constant, and the constant of 0.780 is valid for the temperature of 25°C. Supporting Fig. S5 shows E_{pa} and E_{pc} vs. $\ln v$, where using Eqn. 13 the slopes for E_{pa} and E_{pc} equate to

$RT/2\alpha_a F$ and $-RT/2\alpha_c F$, respectively. The estimated transfer coefficients, $\alpha_a \approx 0.82$ and $\alpha_c \approx 0.79$, indicate a degree of symmetry and confirming a quasi-reversible process [46,55].

The sensor performance in abiotic ASW medium is in good agreement with the reported gold electrode response in an abiotic seawater environment [37]. The analysis for the abiotic ASW medium was supported with a complementary studies into the gold electrode performance in 3.5 wt.% NaCl medium #1 and control ASW test solution (only inorganic species and EDTA - medium #3).

For the three test media (#1, #2 and #3) the gold electrode, polarised between –0.200 V to the plateau at –0.700 V, was able to detect the baseline ORR in a marine environment (Clark electrode). The oxidation reaction of organic components, corresponding to the wave (C'') between +0.500 V to +0.900 V suppress the gold oxidation process beginning around +0.750 V in both #1 and #3 media [46,47,48]. This suggests that more electropositive potentials may be required for the self-cleaning of the gold electrode when immersed in natural seawater enriched with organic components. Likewise, it was demonstrated that inorganic ionic species within ASW medium can diffuse and subsequently electroactively adsorb/desorb on the gold electrode surface, *i.e.,* in the regions (A'') and (B'') at ±0.125 V, and also overall this diffusion dominant process was depressed by the presence of blocking organic components (in the abiotic ASW) adsorbed/desorbed on the gold surface, which in turn represents about 70 % surface coverage. Section 3.4 has outlined a quantitative evaluation of the diffusion process associated with inorganic species (A'') and (B''), showing that the electrochemical response involved was a quasi-reversible process ($\alpha_a \approx 0.82$ and $\alpha_c \approx 0.79$) and was consistent with the redox couple Fe(III)-EDTA/Fe(II)-EDTA. This clearly shows that a conditioning film on the gold surface is not representative of an impermeable and controllable coating but more likely to consist of a monolayer(s) with defects/pinholes facilitating charge diffusion process in analogy with self-assembled monolayers on gold microelectrodes [47,49,56]. Equally, the sorption/desorption of soluble vitamin B redox mediators within the conditioning film will also influence the electrochemical response [25].

3.5. CV for the biotic test condition (*test medium #4*)

Fig. 6a shows the confocal microscopy analysis of the gold electrode after a 72 h immersion in biotic ASW (test medium #4). The bacterial clusters or patchy slime are clearly seen, thus corroborating the presence of bacterial biofilms established under low laminar flow conditions. Using the LCS, a biofilm thickness of 3.0 ± 0.5 μm was measured (Fig. 6b), consistent with the formation of a thin physical diffusion barrier. The electrochemical response for the biotic condition (test medium #4), in contrast with the abiotic ASW (test medium #2), was time-dependent and showed a detectable modification of the electrode kinetics at the gold/biotic ASW interface after a 72 h immersion (Fig. 6c). The CV response for the biotic ASW medium (dashed line, Fig. 6c) was more complex compared to the abiotic medium (solid line in Fig. 5a and Fig. 6c), consistent with [45,57]. Similar to the abiotic ASW (test medium #2), the (A') feature signifies the onset of the gold oxide formation, whereas the corresponding cathodic peak (B') was suppressed indicating an irreversible process [34]. Interestingly, the ORR (C') was more pronounced for the biotic (dashed line) in comparison with the abiotic (solid line), representing higher cathodic current density (in terms of an absolute value) in the presence of *Pseudoalteromonas* bacteria and biofilm formation.
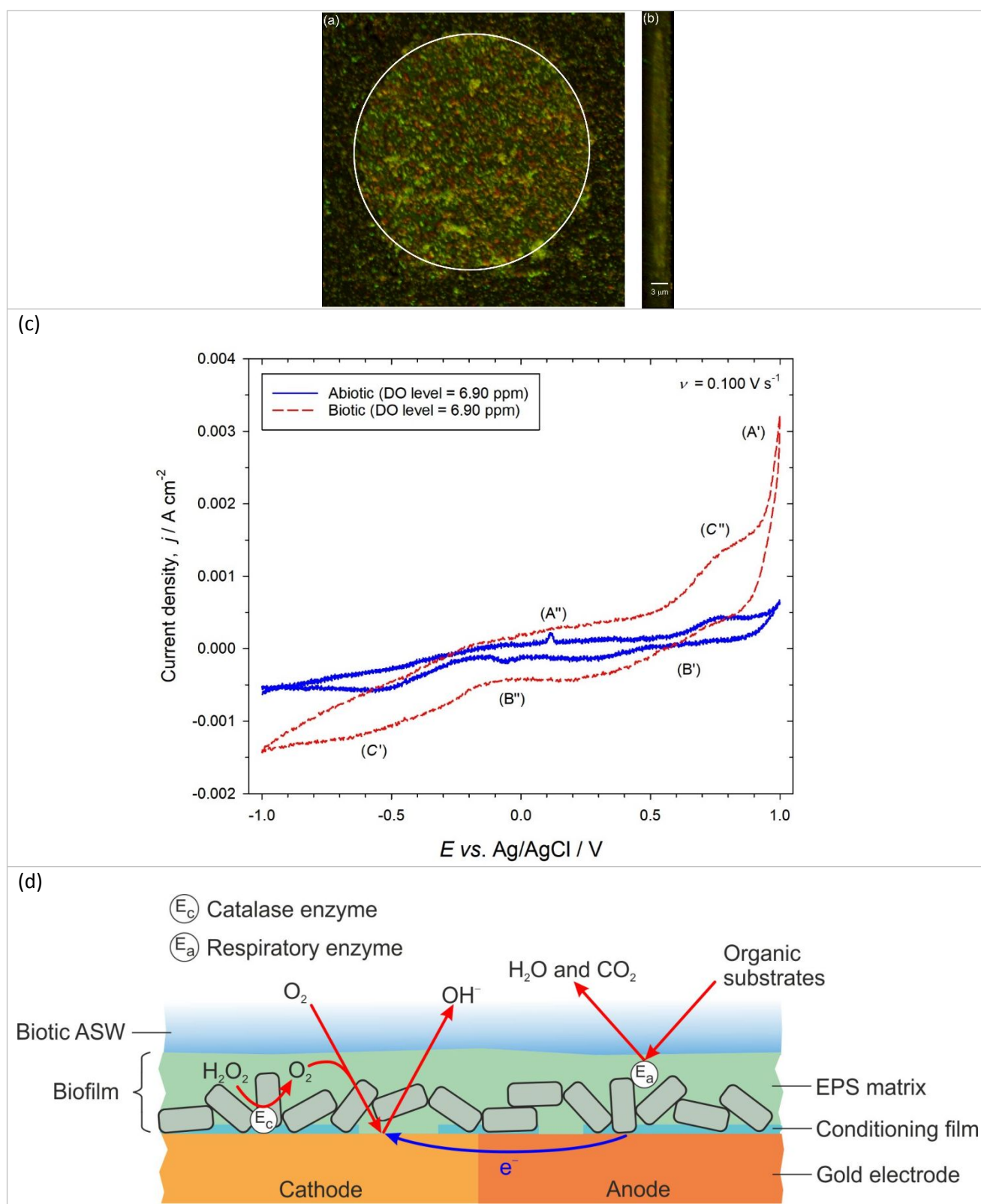
Fig. 6. **(a)** Confocal microscopy of a 72 h-old biofilmed Au electrode stained with the *Bac*Light™ viability kit (white circle outlines the electrode edge) and **(b)** the corresponding cross section. **(c)** Direct comparison of cyclic voltammograms for a 0.2 mm diameter Au electrode in aerated abiotic (test medium #2 – solid line) and biotic ASW (test medium #4 – dashed line) at a scan rate of 0.100 V s^{-1} after 72 h. **(d)** Schematic representation of

electron transfer pathways within a *Pseudoalteromonas* biofilm – typical thickness of the bacterial biofilm is approximately a few microns [3,5,8].

This phenomenon demonstrates an enhancement of the ORR kinetics due to enzymatic activities, which is consistent with [8,11,58,59] where specific enzymes (*e.g.*, catalase) present within the EPS matrix could be responsible for enhanced cathodic currents. The H_2O_2 is decomposed by enzymatic processes to H_2O and O_2, see Eqn. 14. Consequently, a higher oxygen concentration is readily available at the cathode, leading to greater ORR kinetics.

$$2H_2O_2 \xrightarrow{\text{Catalase}} 2H_2O + O_2 \qquad\qquad\qquad ......(14)$$

Conversely, the regions (*A''*) and (*B''*) corresponding to an electroactive adsorption/desorption of inorganic ions were completely absent/overwhelmed when compared with the abiotic condition, associated with hindered diffusion of inorganic ions across the biofilm to the gold surface. This is in good agreement with the aerobic bacteria to change the electrochemical properties of metallic surfaces [8,60]. In addition, a wave in the region (*C''*) was observed between +0.300 to +0.800 V. This wave can be linked to the anodic reaction mechanisms of electroactive *Pseudoalteromonas* biofilms [61,62] and is consistent with previous studies using adhered biofilms on gold surfaces [45,57]. Likewise the broader baseline for the non-faradaic processes is due to diffusion-based EET linked with the migration, diffusion and/or advection of soluble redox mediators through the biofilm EPS matrix, leading to capacitive charging/discharging as charged species move through the biofilm.

From the electrochemical standpoint the various proposed EET mechanisms are all redox mediated (either directly or indirectly); phenazine (electron shuttle) and cytochrome *c* are all redox mediators even if the latter resides within or on the walls of the microorganisms [63,64,65]. When bacterial biofilms develop on the initial conditioning film, a dissolved oxygen concentration gradient is generated (differential aeration cell), leading to the formation of micro-galvanic anode and cathode on the electrode, see Fig. 1c(*ii*). At anodic sites, where dissolved oxygen is deficient, bacteria can oxidise organic components and produce CO_2 plus H_2O [63]. The oxidation reaction at the anode via respiratory enzymes generates electrons collected at the cathodic site where dissolved oxygen is prominent. In this process, bacteria can assist in the electron transfer, where the most active cells can be found at the biofilm/seawater interface [59]. Overall, the enzymatic enhanced ORR via catalase enzymes is the prevailing reaction at cathode sites (Fig. 6d).

The CVs performed in abiotic and biotic ASW media demonstrate that bacterial biofilms change the electrochemical properties at the gold electrode interface, *i.e.*, suppression of regions (*B'*), (*A''*) and (*B''*) and enhance the overall ORR, and also the oxidation of organic material, see Table 5. Herein, the results provide further insights and corroboration of studies conducted by [8,11,45]. By polarising in the negative direction, *i.e.*, between –0.200 V and –0.700 V, the overall and enhanced ORR due to enzymatic processes can be assessed. The working principle of commercialised electrochemical sensors for biofilm sensing relies on similar electrical polarisation methods [3,5,66-69]. With the depression of the gold oxide stripping, the self-cleaning of the biofilmed gold is debatable for a potential range of –1.000 V to +1.000 V, where higher potentials than for the NaCl test solution and ASW medium may be necessary.

Table 5. Summary of detectable electrochemical processes at the Au/biotic ASW interface (Fig. 6c) for a potential range between −1.000 V and +1.000 V (*vs.* Ag/AgCl, 3.5 M KCl)

Potentials	Regions	Description
≥+0.750 V	(*A'*)	Au oxide formation
Around +0.550 V	(*B'*)	N/A
Between −0.200 V to the plateau at −0.700 V	(*C'*)	Enzymatic enhanced ORR wave
±0.125 V	(*A''*)/(*B''*)	N/A
Between +0.500 to +0.900 V	(*C''*)	Enzymatic enhanced oxidation wave for organic material oxidation reaction

4. Conclusions

A once-through flow cell arrangement combined with a 0.2 mm diameter polycrystalline gold electrode for electrochemical investigation has been developed to detect the growth and development of a *Pseudoalteromonas* sp. biofilm within artificial seawater, in order to ascertain the fundamental electrochemical response: Key insights include:

- The gold electrode sensor was fully characterised electrochemically, with marked differences between the abiotic and biotic ASW clearly evident, mainly associated bacterial biofilm surface modification of the interfacial properties with enhanced enzymatic enhanced ORR and oxidation reaction of organic components (undefined redox mediator activity), and suppression of electro-active adsorbed/desorbed inorganic ions due to the biofilm;

- The self-cleaning of a biofilmed gold surface would not be feasible within a operational potential range between −1.000 V and +1.000 V (*vs.* Ag/AgCl, 3M KCl), therefore higher applied potentials than for those observed the NaCl and abiotic ASW media would be required;

- The CV analysis for the biotic ASW demonstrated the significance of polarisation on a biofilmed gold electrode;

- Overall, the influence of organic nutrients under aerated and deaerated, as well as sterile and biotic, conditions have been deconvoluted, thus, allowing the extracellular electron transfer and biofilm responses to be fully assessed. The study demonstrates the importance of differentiating the oxygen reduction kinetics before attributing an aerobic bacterial response involving enzyme and redox mediator activities.

Acknowledgements

Supporting information. Detailed chemical composition of artificial sweater (test medium #2) and control (medium #3); summary of detectable electrochemical processes at the gold/biotic ASW

interface; Pourbaix diagram for the gold-chloride-water system; and schematic and graphical data for determining the anodic and cathodic peak current densities (j_{pa} and j_{pc}) and peak potentials (E_{pa} and E_{pc}) in the voltammograms for the control and abiotic ASW media – idealised plot to illustrate the curve analysis.

References

1. Railkin, A. I. Marine Biofouling: Colonization Processes and Defenses. 1st ed., CRC Press LLC, **2004**. ISBN 0-8493-1419-4.

2. Flemming, H-C.; Sriyutha Murthy, P.; Venkatesan, R.; Cooksey, K.E. Marine and Industrial Biofouling. Springer, **2009**. ISBN 978-3-540-69794-7.

3. Videla, H. A. Manual of Biocorrosion, 1st ed., CRC Press, USA, **1996**. ISBN 0-87371-726-0.

4. Renslow, R.; Babauta, J.; Ivory, C.; Beyenal, H.; Kuprat, A.; Fredrickson, J. Mathematical Modelling of Extracellular Electron Transfer in Biofilms, Biofilms in Bioelectrochemical Systems: From laboratory to data interpretation. 1st ed., edited by H. Beyenal and J. Babauta, John Wiley & Sons, NJ, USA, **2015**. ISBN 978-1-118-41349-4

5. Scotto, V.; Lai, M. E. The Ennoblement of Stainless Steels in Seawater: A Likely Explanation Coming from the Field. *Corros. Sci*. **1998**, 6, 1007-1018. https://doi.org/10.1016/S0010-938X(98)00038-9

6. Donlan, R.M. Biofilms: Microbial Life on Surfaces. *Emerging Infectious Diseases*. **2002**, 8, 881-890. https://dx.doi.org/10.3201/eid0809.020063

7. Flemming, H-C.; Wingender, J.; Griegbe, T.; Mayer, C. Physico-Chemical Properties of Biofilms. In: Evans LV, editor. Biofilms: Recent Advances in their Study and Control. Amsterdam: Harwood Academic Publishers, p. 19–34, **2000**. ISBN-13: 978-9058230935.

8. Bressel, A.; Schultze, J. W.; Khan, W.; Wolfaardt, G. M.; Rohns, H-P.; Irmscher, R.; Schöning, M. J. High Resolution Gravimetric, Optic and Electrochemical Investigations of Microbial Biofilm Formation in Aqueous Systems. *Electrochim. Acta* **2003**, 48, 3363-3372. https://doi.org/10.1016/S0013-4686(03)00406-7

9. Shukla, A. K.; Suresh, P.; Berchmans, S.; Rajendran, A. Biological Fuel Cells and their Applications. *Curr. Sci.* **2004**, 87, 455-468. https://core.ac.uk/download/pdf/34217602.pdf

10. Sutherland, I. W. Biofilm Exopolysaccharides: A Strong and Sticky Framework. *Microbiology* **2001**, 147, 3–9.

11. Busalmen, J. P.; Vázquez, M.; de Sánchez, S. R. New Evidences on the Catalase Mechanism of Microbial Corrosion. *Electrochim. Acta* **2002**, 47, 1857-1865. https://doi.org/10.1016/S0013-4686(01)00899-4

12. Videla, H. A., Herrera, L.K. Understanding Microbial Inhibition of Corrosion. A Comprehensive Review. *International Biodeterioration and Biodegradation*, **2009**, 63, 896-900. https://doi.org/10.1016/j.ibiod.2009.02.002

13. Zuo, R. Biofilms: Strategies for Metal Corrosion Inhibition Employing Microorganism. *Appl. Microbiol. Biot.* **2007**, 76, 1245-1253. https://doi.org/10.1007/s00253-007-1130-6

14. Angelaalincy, M. J.; Navanietha Krishnaraj, R.; Shakambari, G.; Ashokkumar, B.; Kathiresan, S.; Varalakshmi, P. Biofilm Engineering Approaches for Improving the Performance of Microbial Fuel Cells and Bioelectrochemical Systems. *Front. Energy Res.* **2018**, 6. https://doi.org/10.3389/fenrg.2018.00063

15. Astorga, S. E.; Hu, L. X.; Marsili, E., Huang, Y. Electrochemical Signature of *Escherichia coli* on Nickel Micropillar Array Electrode for Early Biofilm Characterisation. *ChemElectroChem*. **2019**, 6, 4674-4680. https://doi.org/10.1002/celc.201901063

16. Torres, C. I.; Marcus, A. K.; Lee, H-S.; Parameswaran, P.; Krajmalnik-Brown, R.; Rittmann, B. E. **2010**. A Kinetic Perspective on Extracellular Electron Transfer by Anode-Respiring Bacteria. *FEMS Microbiol. Rev*. **2010**, 34, 3-17. https://doi.org/10.1111/j.1574-6976.2009.00191.x

17. Tanaka, K.; Yokoe, S.; Igarashi, K.; Takashino, M.; Ishikawa, M.; Hori, K.; Nakanishi, S.; Kato, S. Extracellular

21

Electron Transfer via Outer Membrane Cytochromes in a Methanotrophic Bacterium *Methylococcus capsulatus* (Bath). *Front. Microbiol.* **2018**, 9:2905. https://doi.org/10.3389/fmicb.2018.02905

18. Bos, R.; van der Mei, H.C.; Busscher, H. J. Physico-Chemistry of Initial Microbial Adhesive Interactions –Its Mechanisms and Methods for Study. *FEMS Microbiol. Rev.* **1999**, 23, 179-230. DOI: 10.1111/j.1574-6976.1999.tb00396.x

19. Webb, J. S.; Thompson, L. S.; James, S.; Charlton, T.; Tolker-Nielsen, T.; Koch, B.; Givskov, M.; Kjelleberg, S. Cell Death in *Pseudomanas aeruginosa* Biofilm Development. *J. Bacterio.* **2003**, 185, 4585-4592. https://dx.doi.org/10.1128%2FJB.185.15.4585-4592.2003

20. Bowman, J.P. Bioactive Compound Synthetic Capacity and Ecological Significance of Marine Bacterial Genus *Pseudoalteromonas*. *Mar Drugs* **2007**, 5, 220-241. https://dx.doi.org/10.3390%2Fmd504220

21. Holmström, C.; Kjelleberg, S. Marine *Psuedoalteromonas* Species are Associated with Higher Organisms and Produce Biologically Active Extracellular Agents. *FEMS Microbiology Ecology*, **1999**, 30, 285-293. https://doi.org/10.1111/j.1574-6941.1999.tb00656.x

22. Jing, X.; Liu, X.; Deng, C.; Chen, S.; Zhou, S. Chemical Signals Stimulate *Geobacter soli* Biofilm Formation and Electroactivity. *Biosensors and Bioelectronics* **2019**, 127, 1-9. https://doi.org/10.1016/j.bios.2018.11.051

23. Riegman, R.; Stolte, W.; Noordeloos, A. A. M.; Slezak, D. Nutrurient Uptake and Alkaline (ec 3:1:3:1) Activity of *Emiliania huxleyi* (PRYMNESIOPHYCEAE) During Growth Under *n* and *p* Limitation in Continuous Cultures. *J. Phycol.* **2000**, 36, 87-96. https://doi.org/10.1046/j.1529-8817.2000.99023.x

24. Fletcher, M. The Effects of Culture Concentration and Age, Time, and Temperature on Bacterial Attachment to Polystyrene. Can. *J. Microbiol.* **1977**, 23, 1-6. https://doi.org/10.1139/m77-001

25. Lee, J. S.; Little, B. Yeast extract, Technical Note: Electrochemical and Chemical Complications Resulting from Yeast Extract Addition to Stimulate Microbial Growth. *Corrosion* **2015**, 71, 1434-1440. https://doi.org/10.5006/1833

26. ASTM D1141-98(2013) Standard Practice for the Preparation of Substitute Ocean Water. ASTM International, West Conshohocken, PA, USA, **2013**. www.astm.org/Standards/D1141

27. Kennish, M. J. CRC Practical Handbook of Marine Science, 2nd ed., CRC Press, Boca Raton, FL, USA, **1994**. ISBN 9781138068858.

28. Roszak, D. B.; Colwell, R. R. Survival Strategies of Bacteria in the Natural Environment. *Microbiol. Rev.* **1987**, 51, 365-379. PMID: 3312987

29. Keevil, C. W. Continuous Culture Models to Study Pathogens in Biofilms, Methods in Enzymology: Microbial Growth in Biofilms Part B. **2001**, 337, 104-122. https://doi.org/10.1016/S0076-6879(01)37010-6

30. Rasmussen, K.; Østgaard, K. Adhesion of the Marine Bacterium *Pseudomonas* sp. NCIMB 2021 to Different Hydrogel Surfaces. *Water Res.* **2003**, 37, 519-524. DOI: 10.1016/s0043-1354(02)00306-8

31. Burke, L.D., Nugent, P.F., The Electrochemistry of Gold: I The Redox Behaviour of the Metal in Aqueous Media. *Gold Bull*., **1997**, 30, 43-53. https://doi.org/10.1007/BF03214756

32. Cherevko, S.; Topalov, A. A.; Katsounaros, I.; Mayrhofer, K. J. J. Electrochemical Dissolution of Gold in Acidic Medium, *Electrochem. Commun*., **2013**, 28, 44-46. https://doi.org/10.1016/j.elecom.2012.11.040

33. Juodkazis, K.; Juodkazytė, J.; Jasulaitienė, V.; Šebeka, B. XPS Studies on the Gold Oxide Surface Layer Formation, *Electrochem. Commun*. **2000**, 2, 503-507. https://doi.org/10.1016/S1388-2481(00)00069-2

34. Ling, Y.; Elkenbracht, J. C.; Flanagan, W. F.; Lichter, B. D. The Electrochemical Oxidation of Gold in 0.6 M NaCl and 0.3 M Na_2SO_4 Solutions. *J. Electrochem. Soc.* 1997, **144**, 2689-2697. https://doi.org/10.1149/1.1837883

35. Shao, M.H.; Adzic, R. R. Spectroscopic Identification of the Reaction Intermediates in Oxygen Reduction on Gold in Alkaline Solutions, *J. Phys. Chem. B* **2005**, 109, 16563-16566. https://doi.org/10.1021/jp053450s

22

36. Vassilev, P; Koper, M. T. M. Electrochemical Reduction of Oxygen on Gold Surfaces: A Density Functional Theory Study of Intermediates and Reaction Paths. *J Phys Chem. C* **2007**, 111, 2607-2613. https://doi.org/10.1021/jp064515

37. Andoralov, V. M.; Tarasevich, M. R.; Tripachev, O. V. Oxygen Reduction Reaction on Polycrystalline Gold. Pathways of Hydrogen Peroxide Transformation in the Acidic Medium. *Russian J. Electrochem.* **2011**, 47, 1327-1336. https://doi.org/10.1134/S1023193511120020

38. Ge, X.; Sumboja, A.; Wuu, D.; An, T.; Li, B.; Goh, F. W. T.; Hor, T. S. A.; Zong, Y.; liu, Z. Oxygen Reduction in Alkaline Media: From Mechanisms to Recent Advances of Catalysts. *ACS Catal.* **2015**, 5, 4643-4667. https://doi.org/10.1021/acscatal.5b00524

39. Jusys, Z.; Behm. R. J., The Effect of Anions and pH on the Activity and Selectivity of an Annealed Polycrystalline Au Film Electrode in the Oxygen Reduction Reaction-Revisited. *ChemPhysChem* **2019**, 20, 3276-3288. https://doi.org/10.1002/cphc.201900960

40. Pletcher, D.; Walsh, F. Industrial Electrochemistry. 2nd ed., The Electrochemical Consultancy, UK, **1993**. ISBN 0 412 30410 4.

41. Walsh, F. 1993. A First Course in Electrochemical Engineering. 1st ed., The Electrochemical Consultancy, UK, **1993**. https://doi.org/10.1002/aic.690420437

42. Denuault, G. Electrochemical Techniques and Sensors for Ocean Research. *Ocean Sci.* **2009**, 5, 697-710. https://doi.org/10.5194/os-5-697-2009

43. Sosna, M.; Denuault, G.; Pascal, R.W.; Prien, R.D.; Mowlem, M. Development of a Reliable Microelectrode Dissolved Oxygen Sensor. *Sens. Actuator* B-*Chem.* **2007**, 123, 344-351. DOI: 10.1016/j.snb.2006.08.033

44. Sosna, M.; Denuault, G.; Pascal, R. W.; Prien, R. D.; Mowlem, M. Field Assessment of a New Membrane-Free Microelectrode Dissolved Oxygen Sensor for Water Column Profiling. *Limnol. Oceanogr.: Methods* **2008**, 6, 180-189. https://doi.org/10.4319/lom.2008.6.180

45. Hu, Y.; Zhang, J.; Ulstrup, J. Interfacial Electrochemical Electron Transfer Processes in Bacterial Biofilm Environments on Au(111). *Langmuir* **2010**, 26, 9094-9103. https://doi.org/10.1021/la9047853

46. Bard, A. J.; Faulkner, L. R. Electrochemical Methods: Fundamentals and Applications. 2nd ed., John Wiley and Sons, USA, **2004**. ISBN 0-471-04372-9.

47. Davis, K. L.; Drews, B. J.; Yue, H.; Waldeck, D. H.; Knorr, K.; Clark, R. A. Electron-Transfer Kinetics of Covalently Attached Cytochrome c/SAM/Au Electrode Assemblies. *J. Phys. Chem. C* **2008**, 112, 6571-6576. https://doi.org/10.1021/jp711834t

48. Sheffer, M.; Vivier, V.; Mandler, D. Self-Assembled Monolayers on Au Microelectrodes. *Electrochem. Commun.* **2007**, 9, 2827-2832. https://doi.org/10.1016/j.elecom.2007.10.008

49. Moulton, S. E.; Barisci, J. N.; Bath, A.; Stella, R.; Wallace, G. G. Studies of Double Layer Capacitance and Electron Transfer at a Gold Electrode Exposed to Protein Solutions. *Electrochim. Acta* **2004**, 49, 4223-4230. https://doi.org/10.1016/j.electacta.2004.03.034

50. Gamby, J.; Pailleret, A.; Clodic, C. B.; Pradier, C-M.; Tribollet, B. *In situ* Detection and Characterisation of Potable Biofilms on Materials by Microscopic, Spectroscopic and Electrochemistry Methods. *Electrochim. Acta* **2008**, 54, 66-73. https://doi.org/10.1016/j.electacta.2008.07.018

51. Barus, C.; Gros, P.; Comtat, M.; Daunes-Marion, S.; Tarroux, R. Electrochemical Behaviour of N-acetyl -L-Cysteine on Gold Electrode – A Tentative Reaction. *Electrochim. Acta* **2007**, 52, 7978-7985. https://doi.org/10.1016/j.electacta.2007.06.065

52. Shimizu, K.; Hutchinson, R.; Engelmann, M. D.; Francis Cheng, I. Cyclic Voltammetric and Aqueous Equilibria Model Study of the pH Dependant Iron(II/III) Ethylenediamminetetraacetate Complex Reduction Potential.

J. Electroanal. Chem. **2007**, 603, 44-50. https://doi.org/10.1016/j.jelechem.2007.01.027

53. Straub, K. L.; Benz, M.; Schink, B. Iron Metabolism in Anoxic Environments at Near Neutral pH. *FEMS Microbiol. Ecol.* **2001**, 34, 181-186. https://doi.org/10.1111/j.1574-6941.2001.tb00768.x

54. Wang, Z.; Liu, C.; Wang, X.; Marshall. M. J.; Zachara, J. M.; Rosso, K. M.; Dupuis, M.; Fredrickson, J. K.; Heald, S.; Shi, L. Kinetics of Reduction of Fe(III) Complexes by Outer Membrane Cytochromes MtrC and OmcA of *Shewanella oneidensis* MR-1. *Appl. Environ. Microb*. **2008**, 74, 6746-6755. doi:10.1128/AEM.01454-08

55. Guidelli, R.; Compton, R. G.; Feliu, J. M.; Gileadi, E.; Lipkowski, J.; Schmickler, W.; Tasatti, S. Defining the Transfer Coefficient in Electrochemistry: An assessment (IUPAC Technical Report). *Pure Appl. Chem*. **2014**, 86, 245-258. https://doi.org/10.1515/pac-2014-5026

56. Huang, C-H.; McClenaghan, N. D.; Kuhn, A.; Bravic, G.; Bassani, D. M. Hierarchical Self-Assembly of All-Organic Photovoltaic Devices. *Tetrahedron* **2006**, 62, 2050-2059. https://doi.org/10.1016/j.tet.2005.09.150

57. Busalmen, J. P.; Berná, A.; Feliu, J. M. Spectroelectrochemical Examination of the Interaction Between Bacteria Cells and Gold Electrodes. *Langmuir* **2007**, 23, 6459-6466. https://doi.org/10.1021/la700406q

58. Beech, I. B.; Sunner, J. Biocorrosion: Towards Understanding Interactions Between Biofilms and Metals. *Curr. Opin. Biotechnol.* **2004**, 15, 181-186. DOI: 10.1016/j.copbio.2004.05.001

59. Nercessian, D.; Duville, F.B.; Desimone, M.; Simison, S.; Busalmen, J. P. Metabolic Turnover and Catalase Activity of Biofilms of *Pseudomanas fluorescens* (ATCC 17552) as Related to Copper Corrosion. *Water Res.* **2010**, 44, 2592-2600. https://doi.org/10.1016/j.watres.2010.01.014

60. Tribollet, B. Electrochemical Sensors for Biofilm and Biocorrosion. *Mater. Corros.* **2003**, 54, 527-534. https://doi.org/10.1002/maco.200390116

61. Dulon, S.; Parot, S.; Delia, M-L.; Bergel, A. Electroactive Biofilms: New Means for Electrochemistry. *J. Appl. Electrochem*. **2007**, 37, 173-179. https://doi.org/10.1007/s10800-006-9250-8

62. Busalmen, J. P.; de Sánchez, S. R. Changes in the Electrochemical Interface as a Result of the Growth of *Pseudomonas fluorescens* Biofilms on Gold. *Biotechnol. Bioeng.* **2002**, 82, 619-624. DOI: 10.1002/bit.10600

63. Zhao, F.; Slade, R. C. T.; Varcoe, J. R. Techniques for the Study and Development of Microbial Fuel Cells: An Electrochemical Perspective. *Chem. Soc. Rev.* **2009**, 38, 1926-1939. https://doi.org/10.1039/B819866G

64. Blackwood, D. J. An Electrochemist Perspective of Microbiologically Influenced Corrosion. *Corrosion and Materials Degradation*, **2018**, 1, 59-76. doi: 10.3390/cmd1010005

65. Pandit, S.; Chandrasekhar, K.; Kakarla, R.; Kadier, A.; Jeevitha, V. Basic Principles of Microbial Fuel Cell: Technical Challenges and Economic Feasibility. In Microbial Applications; Kalia, V., Kumar, P., Eds.; Springer: Cham, Switzerland, **2017**, 1, pp. 165–188. https://doi.org/10.1007/978-3-319-52666-9_8

66. Bruijs, M. C. M.; Venhuis, L. P.; Jenner, H. A.; Licina, G. J.; Daniels, D. Biocide Optimisation Using an On-Line Biofilm Monitor. *Power Plant Chemistry* **2001**, 3, 400-405.

67. Cristiani, P. Solutions to Fouling in Power Station Condensers. *Appl. Therm. Eng.* **2005**, 25, 2630-2640. https://doi.org/10.1016/j.applthermaleng.2004.11.029

68. Salta, M.; Wharton, J. A.; Stoodley, P.; Dennington, S. P.; Goodes, L. R.; Werwinski, S.; Mart, U.; Wood, R. J. K.; Stokes, K. R. Designing Biomimetic Antifouling Surfaces. *Philos. Trans. R. Soc.* **2010**, 368, 4729-4754. https://doi.org/10.1098/rsta.2010.0195

69. Sedki, M.; Hassan, R. Y. A.; Andreescu, S.; El-Sherbiny, I. M. Online-Monitoring of Biofilm Formation Using Nanostructured Electrode Surfaces. *Mater. Sci. Eng. C* **2019**, 100, 178-185. https://doi.org/10.1016/j.msec.2019.02.112

24

1
2
3 **For Table of Contents Only**
4
5
6
7
8
9
10
11
12
13
14
15
16
17
18
19
20
21
22
23
24
25
26
27
28
29
30
31
32
33
34
35
36
37
38
39
40
41
42
43
44
45
46
47
48
49
50
51
52
53
54
55
56
57